

**Title:**

Discrete Adaptive Zone Light Elements (DAZLE): A New Approach to Adaptive Imaging

**Authors:**

Robert L. Kellogg<sup>a</sup> and Michael J. Escuti<sup>b</sup>

**Affiliation:**

<sup>a</sup>Argon ST Inc., 12701 Fair Lakes Circle, Suite 800, Fairfax, VA (USA)

<sup>b</sup>North Carolina State University, Dept Electrical & Computer Engineering, Raleigh, NC (USA)

**Presented At:**

*SPIE Optics & Photonics Conference*, San Diego, CA (August 30, 2007)

**Citation:**

R.L. Kellogg and M.J. Escuti, "Discrete Adaptive Zone Light Elements (DAZLE): A New Approach to Adaptive Imaging", *Proceedings of SPIE*, vol. **6714**, no. 67140H (2007).

Copyright 2007 Society of Photo-Optical Instrumentation Engineers.

This paper was published in Proceedings of SPIE Vol. 6714 and is made available as an electronic reprint with permission of SPIE. One print or electronic copy may be made for personal use only. Systematic or multiple reproduction, distribution to multiple locations via electronic or other means, duplication of any material in this paper for a fee or for commercial purposes, or modification of the content of this paper are prohibited.

# Discrete Adaptive Zone Light Elements (DAZLE): A New Approach to Adaptive Imaging

Robert L. Kellogg<sup>a</sup> and Michael J. Escuti<sup>b1</sup>

<sup>a</sup>Argon ST Inc., 12701 Fair Lakes Circle, Suite 800, Fairfax, VA (USA)

<sup>b</sup>North Carolina State University, Department of Electrical and Computer Engineering, Raleigh, NC (USA)

## ABSTRACT

New advances in Liquid Crystal Spatial Light Modulators (LCSLM) offer opportunities for large adaptive optics in the midwave infrared spectrum. A light focusing adaptive imaging system, using the zero-order diffraction state of a polarizer-free liquid crystal polarization grating modulator to create millions of high transmittance apertures, is envisioned in a system called DAZLE (Discrete Adaptive Zone Light Elements). DAZLE adaptively selects large sets of LCSLM apertures using the principles of coded masks, embodied in a hybrid Discrete Fresnel Zone Plate (DFZP) design. Issues of system architecture, including factors of LCSLM aperture pattern and adaptive control, image resolution and focal plane array (FPA) matching, and trade-offs between filter bandwidths, background photon noise, and chromatic aberration are discussed.

**Keywords:** adaptive imaging, coded aperture mask, Fresnel zone plate, midwave infrared, liquid crystals, spatial light modulator, polarization-independence, polarization grating

## 1. INTRODUCTION – DAZLE CONCEPT

The Defense Advanced Research Projects Agency (DARPA) under a Broad Agency Announcement (BAA-06-11) solicited ideas to develop and demonstrate large-area addressable masks for adaptive coded aperture imaging systems operating in the midwave infrared (MWIR). The purpose was to establish simple, lightweight, and extremely wide field of view systems traditionally not possible without the expense of large, compound optical systems. Argon ST, Inc. and a consortium of universities (North Carolina State University and Southern Methodist University), contractors (BAE Systems and Boulder Nonlinear), and consultants (Fennimore and Palmer) responded to the challenge.

Using DARPA requirements<sup>1</sup>, we examined a concept for wide-area surveillance using a coherent MWIR system that employs adaptive phase-array steering of incoming radiation using a Discrete Adaptive Zone Light Element (DAZLE). The principle of operation is based on coherent apertures created by the zero-order diffraction of a high-efficiency Liquid Crystal Spatial Light Modulator (LCSLM). The original system concept was based on Modified Uniformly Redundant Arrays (MURA)<sup>2,3</sup> coded apertures that have been used in  $x$ -ray and  $\gamma$ -ray astronomy.

MURA coded apertures create shadowcasts that can be transformed into images by deconvolution (Figure 1). MURA imaging works on both discrete and continuously distributed light sources, as confirmed by our computer simulations. The focal FPA image can be reconstructed by deconvolution using an anti-mask defined as  $G = 2A - 1$ , where  $A$  is the coded mask pattern. An example of cyclic code deconvolution (Figure 2) is demonstrated with the famous “Lena” portrait.

---

<sup>1</sup> Correspondence should be addressed to: robert.kellogg@argonst.com and/or mjescuti@ncsu.edu

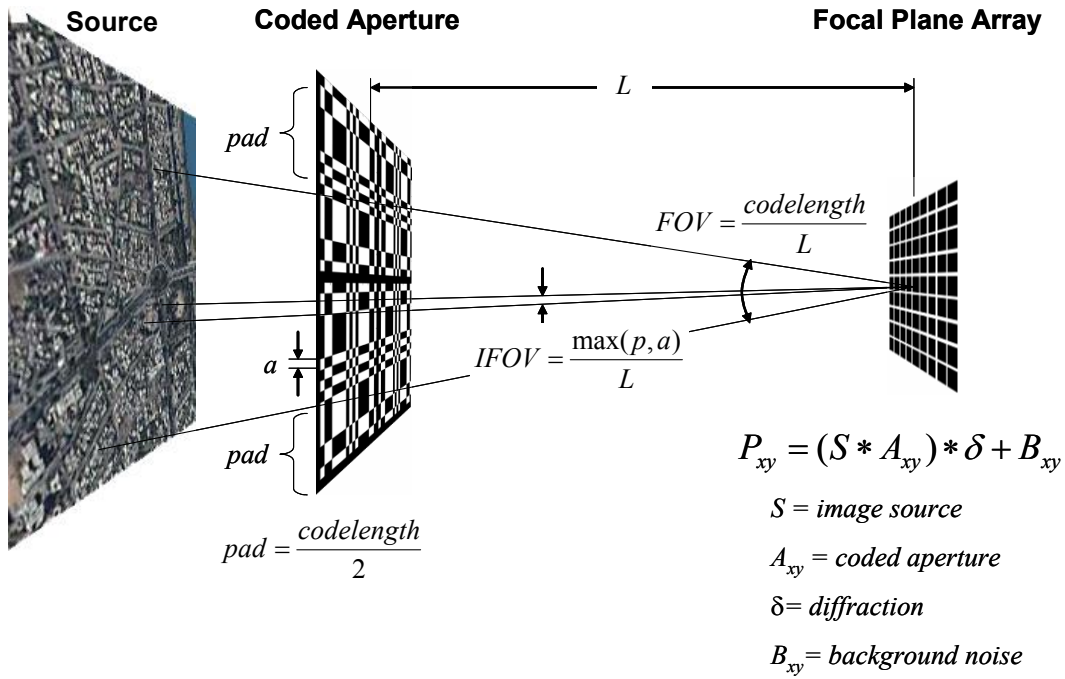


**Figure 1** Image Forming by Modified Uniformly Redundant Arrays (MURA)

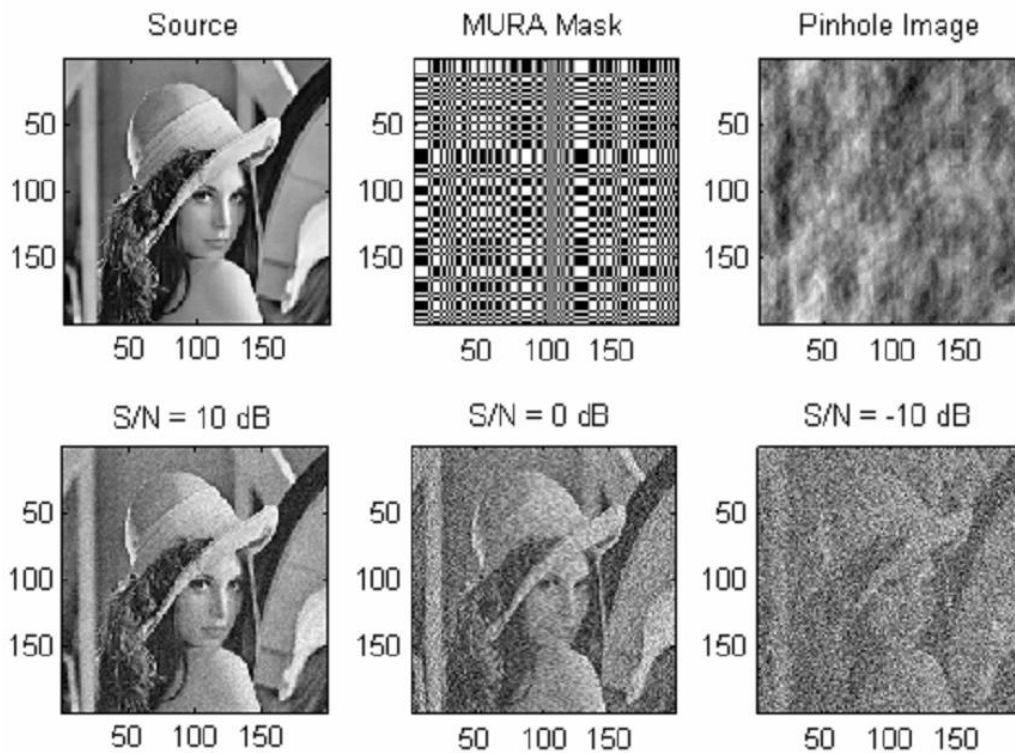


**Figure 2** (Top Row) Original image, MURA mask, and noiseless shadowcast on a focal plane array. (Bottom Row) Shadowcast reconstruction by deconvolution under the presence of 10dB, 0dB, and -10dB signal to noise ratio (SNR).

Unfortunately, the MWIR wavelength ( $\sim 4 \mu\text{m}$ ) has unacceptable edge-diffraction not present in  $x$ -ray and  $\gamma$ -ray imaging. A single  $50 \mu\text{m}$  pinhole aperture with a 5-cm focal length creates a diffraction spot 8 mm in diameter. Light from this *single* aperture would cover nearly an entire  $20 \mu\text{m}$  pitch  $1024 \times 1024$  MWIR FPA. Therefore, classical MURA imaging is untenable without additional lenses due to the blurring effect of diffraction.

A viable alternative involves *coherent* adaptive optics such that small pinhole openings act in unison. Classically this has been restricted to apertures such as the Fresnel Zone Plate (FZP) using alternating rings of transparent and opaque material. The evolution of a FZP into the DAZLE coded aperture will be discussed in Section 3. Regardless of the details of the design, it is essential to have an array of apertures composed of a modulator technology that is photon-efficient, fast, and addressable (at MWIR wavelengths). We have therefore examined a polarizer-free, transmissive, liquid crystal technology, which is being developed at NCSU, as a compelling basis for the spatial light modulator (SLM) in DAZLE.

## 2. POLARIZATION-INDEPENDENT LIQUID CRYSTAL MODULATOR

The LCSLM described here can deliver high contrast ratio (400:1) switching of unpolarized light for efficient, low power “on/off” state modulation. This polarizer-free modulator is based on a switchable anisotropic hologram known as a *liquid crystal polarization grating* (LCPG).<sup>4-9</sup> This switchable anisotropic diffractive element is composed of a bulk nematic LC with a continuous periodic birefringence profile (i.e.  $\mathbf{n}(x) = [\sin(\pi x/\Lambda), \cos(\pi x/\Lambda), 0]$ ), as shown in Figure 3. It can be made in switchable or polymeric materials, and while it has so far been widely reported in the transmissive configuration, implementing a reflective mode is also possible. Its basic function is that light passing through the grating structure is diffracted according to the simple functions listed in the first two rows of Table 1. At zero applied voltage, it is possible to have all light (regardless of input polarization) diffract into *just* the  $\pm 1$ -orders (Figure 3 (b) and (d)), while an applied voltage greater than a voltage threshold will re-orient the LC director out of the plane, effectively erasing the grating and allowing the incident light to pass directly through (Figure 3 (c) and (e)). In essence, the analog modulator couples light between the 0- and  $\pm 1$ -orders. Note that initial simulations<sup>6,10</sup> suggest it is important to have at least four grating periods  $\Lambda$  of the PG within each pixel.

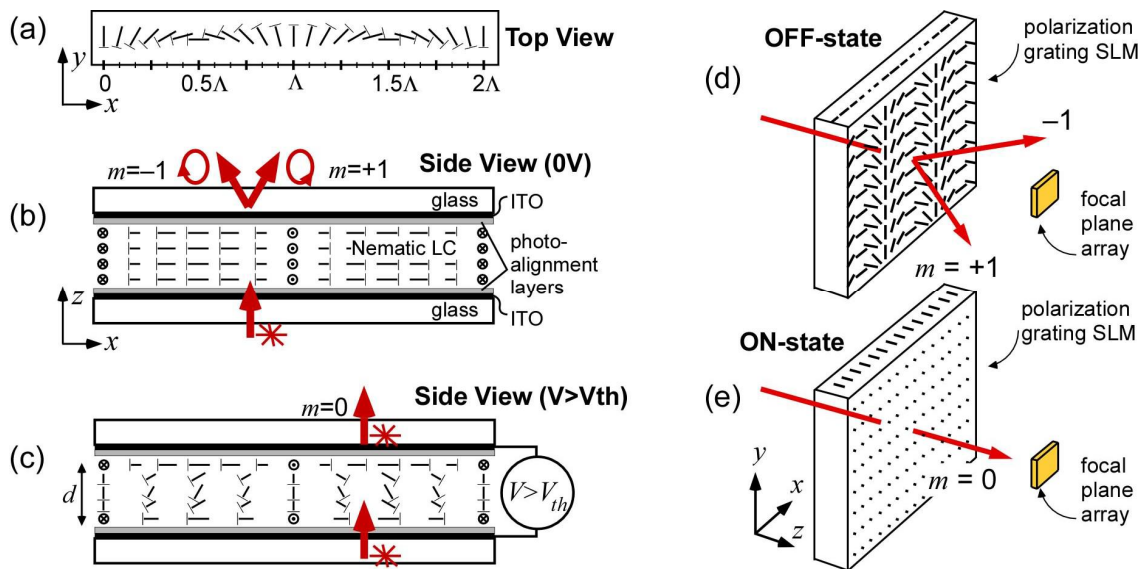


**Figure 3** The polarization independent SLM at the pixel level: (a) Basic geometry (top view); (b) Basic geometry (side view) and illustrated diffraction behavior when  $\Delta nd = \lambda/2$  with zero applied voltage – note that only the  $\pm 1$ -orders are ideally present regardless of input polarization; (c) Diffraction behavior when the applied voltage exceeds  $V_{th}$  – note that light increasingly couples into the zero-order, and eventually the PG is reversibly “erased”; (d) Operation of the SLM with the focal plane array when pixel is “OFF” and (e) when pixel is “ON”. Note that illustrations are not drawn to scale.

The LC-PG modulator is concurrently being developed at NCSU for high-efficiency LC micro-display applications<sup>11,12</sup> (at visible wavelengths), with partial support from the National Science Foundation and the startup-company ImagineOptix Inc. Near-IR operation of a polymer version of the same diffraction grating has been experimentally proven for spectro-polarimetry<sup>5</sup> applications, and more recently an achromatic version with a slightly different structure was demonstrated<sup>13</sup> with high diffraction efficiency (> 99%) over the entire visible range of wavelengths. In this Section, we will discuss its fundamental properties, and estimate its potential and limitations at the MWIR wavelengths of interest to the DAZLE design.

This little-known class of periodic structures (sometimes called vectorial gratings) has actually been around since the 1970s<sup>14</sup>. Conventional diffraction gratings and holograms operate by periodically modulating the phase or amplitude of light propagating through them. Polarization gratings<sup>15</sup> (PGs) instead operate by modulating the polarization state of light passing through, and are embodied as a spatially varying birefringence and/or dichroism. It was recognized early<sup>15,16</sup> that PGs manifest a combination of the advantageous properties of both thick-and thin-gratings. Related to the DAZLE application, the following LCPG properties are notable:

- Diffraction occurs into *no more than three orders* (zero and  $\pm$ first);
- All orders, including the zero-order, can have *~100% to ~0% diffraction efficiency* depending on the retardation ( $\Delta n d / \lambda$ );
- Zero-order transmittance *does not depend on polarization*;
- Contrast of the modulator depends only on the formation of the grating, and *does not involve polarizers*;
- Comparatively wide bandwidth (similar to thin gratings).

The basic optical, elastic, and electrical properties are summarized in Table 1, where  $\{K_{11}, K_{22}, K_{33}\}$  are the {splay, twist, bend} elastic constants. A detailed analysis of the optical<sup>6</sup> behavior, the LC-elastic<sup>17</sup> behavior, and modulator design rules<sup>7</sup> is available. In short, for a MWIR wavelength ( $\lambda \sim 4 \mu\text{m}$ ) and current nematic LC materials (birefringence  $\Delta n \sim 0.3$ ), the modulator offers *~100% peak transmittance* (aside from electrode absorption), switching times of *~20 ms*, minimum aperture size of *~50  $\mu\text{m}$* , and operating voltages of  $\leq 20$  Vrms. These nematic switching times are the same or better than conventional LC based SLMs optimized for MWIR. If a ferroelectric LC version of the PG can be developed, the switching times should be even faster, likely  $\leq 2$  ms. However, the switching speeds of the LCPG at low temperatures (e.g.  $\leq 275^\circ\text{K}$ ) with any LC have not yet been investigated.

**Table 1** Optical, Elastic, and Electrical Properties of LCPGs ( $\Delta n = 0.3$ )

	<b>Property</b>	<b>Typical Values for MWIR</b> ( $\lambda_{\text{max}} = 4 \mu\text{m}$ )
0-order Diffraction Efficiency	$\eta_0 = \cos^2\left(\frac{\pi\Delta n d}{\lambda}\right)$	~0 to ~100%, aside from electrode losses
Sum of $\pm 1$ -order Diffraction Efficiency	$\Sigma\eta_{\pm 1} = \sin^2\left(\frac{\pi\Delta n d}{\lambda}\right)$	~0 to ~100%, aside from electrode losses
Separation Angle Btwn Diffraction Orders ( $^\circ$ )	$\theta = \sin^{-1}\left(\frac{\lambda}{\Lambda}\right)$	~ 20-30 $^\circ$
LC Layer Thickness	$d = \frac{\lambda_{\text{max}}}{2\Delta n}$	~ 6-7 $\mu\text{m}$
Grating Period ( $\Lambda$ )	$\Lambda > \frac{\lambda_{\text{max}}}{2\Delta n} \sqrt{2 - \frac{K_{22}}{K_{11}}}$	~ 8-15 $\mu\text{m}$
Minimum Aperture Size	$\geq 4\Lambda$	$\geq 32$ -60 $\mu\text{m}$
Threshold Voltage	$V_{th} = \pi \sqrt{\frac{K_{11}}{\epsilon_0 \Delta \epsilon}} \left(1 - \frac{d^2}{d_c^2}\right)$	< 2 Vrms
Operating Voltage	–	~ 0-20 Vrms
Critical Thickness	$d_c = \frac{\Lambda}{\sqrt{2 - \frac{K_{22}}{K_{11}}}}$	~ $\Lambda/2$ (typ. few $\mu\text{m}$ )
Switching Times	$\tau_{off} + \tau_{on} \approx \frac{\gamma_1^* d^2}{\epsilon_0 \Delta \epsilon V_{th}^2}$	$\tau_{off} + \tau_{on} \approx 2 - 20$ ms

We find excellent agreement between our experimental results of transmission spectra/switching and Table 1. The following fabrication<sup>4,8</sup> was used for the representative results reported here. Standard InTiO-glass and 2  $\mu\text{m}$  spacers (within the glue seal) formed the cell. We used the photo-alignment layer<sup>18</sup> ROP201 (Rolic) and the liquid crystal MLC-6080 (Merck,  $\Delta n = 0.202$ ,  $T_{\text{NI}} = 95^\circ\text{C}$ ), and a grating period of  $\Lambda = 11 \mu\text{m}$ . All electro-optic measurements were done with a 5 kHz square wave (with 0 V bias).

Basic switching behavior is shown in Figure 4. The transmittance vs. voltage was measured using a HeNe (633 nm) laser, and revealed a contrast of  $\sim 380:1$  for the 0-order. Note that  $V_{\text{th}} = 1.65 \text{ V}$  for this sample. Additionally, transmission spectra with unpolarized input light were acquired with a spectrophotometer at several applied voltages. The switching times of this sample are around 2 ms, as shown in Figure 4(c). The maximum transmittance of the 0<sup>th</sup>-order approaches 100%, which is approximately double the efficiency of almost all other liquid crystal SLMs because it is polarization independent.

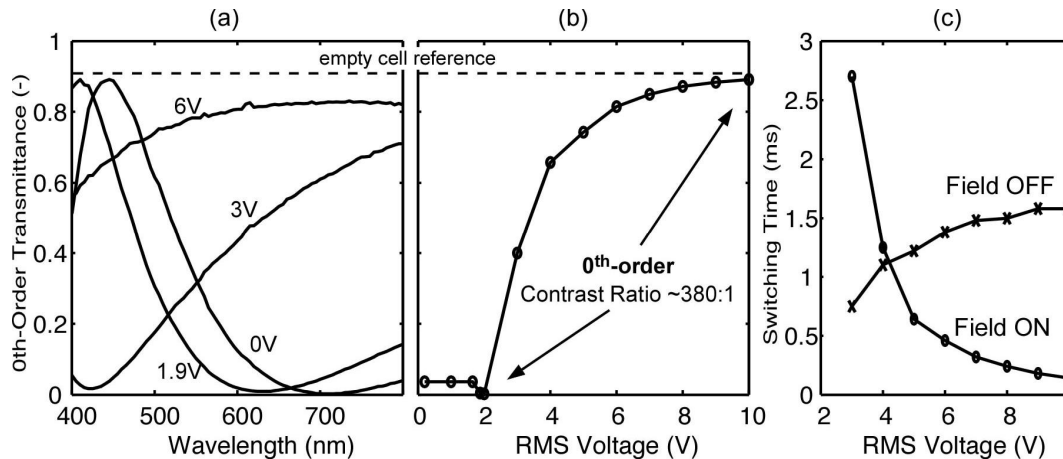


**Figure 4** Measured transmission properties of a representative sample optimized for projection display applications: (a) Spectral response to applied voltage – notice that the transmission minimum shifts to smaller wavelengths as voltage increases; (b) Transmission vs. voltage characteristic, measured with a linearly polarized, laser input (HeNe, 633 nm) – note that both  $\eta_0$  and  $\Sigma\eta_{\pm 1}$  were experimentally found to be polarization independent; (c) Full contrast switching times. ( $\Lambda = 11 \mu\text{m}$  and  $d = 2.0 \mu\text{m}$ )

We have also studied the combination of the polarization independent LCPG with a pinhole aperture array with a Finite-Difference Time-Domain (FDTD) software called WOLFSIM<sup>19</sup>. In this way, we are modeling the whole LCSLM with a tool developed for arbitrary anisotropic structures. Note that the parameters used here are not optimized and are only intended to show the principle of operation. We first calculated the near-field pattern of a simple 50  $\mu\text{m}$  pinhole aperture (shadow mask) without the modulator, as shown in Figure 5(a) for 4  $\mu\text{m}$  light. The Fraunhofer far-field pattern was also calculated at a distance of 5 cm away from the pinhole, and as expected the aperture creates diffraction that exactly corresponds to the analytic expression (the  $\text{sinc}^2(\dots)$  function) with a width of  $\sim 8 \mu\text{m}$ . We then modeled the SLM (in the “OFF” state) on top of the same pinhole aperture, as shown in Figure 5(b). Light in this case is diffracted by the grating as well as the aperture, and most of the light in an oblique direction. Finally, we explored the possibility of removing the pinhole aperture shadow mask and letting the SLM in its “OFF” state block the light from the detector and turn “ON” only a 50  $\mu\text{m}$  region. As shown in Figure 5(c), this results in a similar pattern (red) as with the shadow mask aperture (blue) surrounded by bright oblique lobes that contain the “blocked” rays. In short, it should be possible to directly implement the pinhole aperture array element by patterning the SLM electrodes.

LCSLM can be extended into the MWIR. The theoretical contrast ratio for the LCPG is infinity for a spectrally narrow light source. Experiments, of course, show a finite contrast ratio. Our work at visible wavelengths has so far shown a maximum contrast ratio for the zero-order is consistently around 400:1. Recent unpublished work at near-IR wavelengths (laser around 1.55  $\mu\text{m}$ ) resulted in the same range, where the maximum attenuation was around  $-30$  to  $-34$  dB (similar results in Ref.<sup>5</sup>). All of the above results also show  $\geq 99\%$  peak transmittance, aside from Fresnel interface reflections and absorption losses in electrode/glass. We therefore anticipate similar performance at MWIR wavelengths.

In short, the polarization independent LCSLM described here offers the inherent advantage of double the brightness and faster switching as compared to almost all other LC modulators, while maintaining similar switching voltages, cell thickness, contrast ratios, and materials.

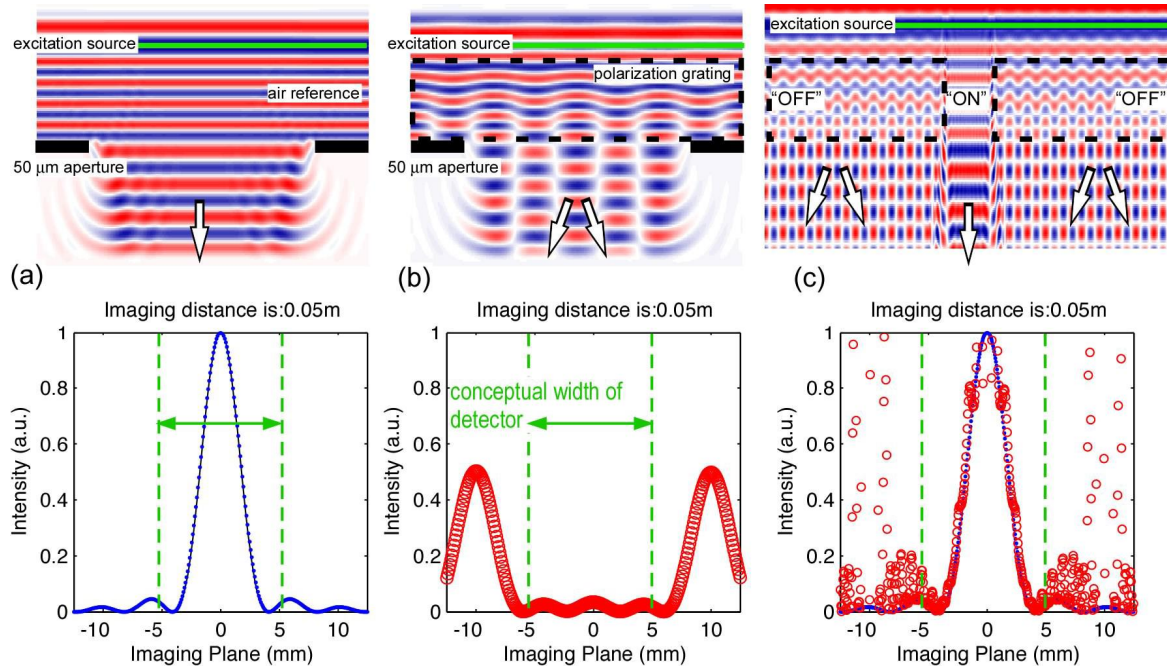


**Figure 5** FDTD simulations at  $\lambda = 4 \mu\text{m}$  with  $50 \mu\text{m}$  apertures (near-field (top) and Fraunhofer far-field (bottom)), using the software WOLFSIM<sup>19</sup>: (a) A simple pinhole aperture (for reference) implemented as an absorbing shadow mask; (b) With the SLM on top of the same pinhole aperture; (c) The pinhole aperture created directly by the SLM with the shadow mask. While linearly polarized input light was used for this simulation, the results are the same regardless of its orientation (e.g. TE and TM response are identical) – therefore this is valid for unpolarized light.

### 3. DAZLE PERFORMANCE REQUIREMENTS FOR A SPATIAL LIGHT MODULATOR

The underlying principle of coherent addition can be used to reduce diffraction blurring. A special class of aperture spacing called Minimum Redundancy Arrays<sup>20</sup> (MRA) was investigated through simulations by NSCU for applicability to LCSLM. Using Finite Difference Time Domain (FDTD) calculations, the far field diffraction pattern was determined for an array of four controllable  $50 \mu\text{m}$  LCSLM apertures with  $50 \mu\text{m}$  spacing. Using the same MWIR parameters of wavelength and focal length, FDTD analysis of the single  $50 \mu\text{m}$  aperture created a diffraction spot 8-mm in diameter, consistent with classical diffraction theory (Figure 6(a)). Two apertures created the classic Young’s double slit response (Figure 6(b)). Finally, an MRA aperture pattern [110101] (where the first two apertures merge into an opening  $100 \mu\text{m}$  across followed by alternating closed and open apertures of  $50 \mu\text{m}$  each) was examined (Figure 6(c)), and as expected, an even smaller diffraction spike less than 1 mm diameter is created with extremely low side lobe photon splatter.

There are many known linear and 2D MRA patterns, and we believe that it is possible to merge the principles of MRA pattern generation with other approaches that create discrete, semi-randomized apertures. For example, new FZP aperture designs<sup>21,22</sup> show that pinhole aperture arrays can be designed for improved diffraction focusing with photon efficiency. There also appear to be approaches to broadening the wavelength band of the FZP, including the introduction of LCSLM optical path length gradients<sup>23,24</sup>, pinhole shaping<sup>25</sup>. The issue of wavelength band coherency will be addressed in the next section discussing System Implementation.

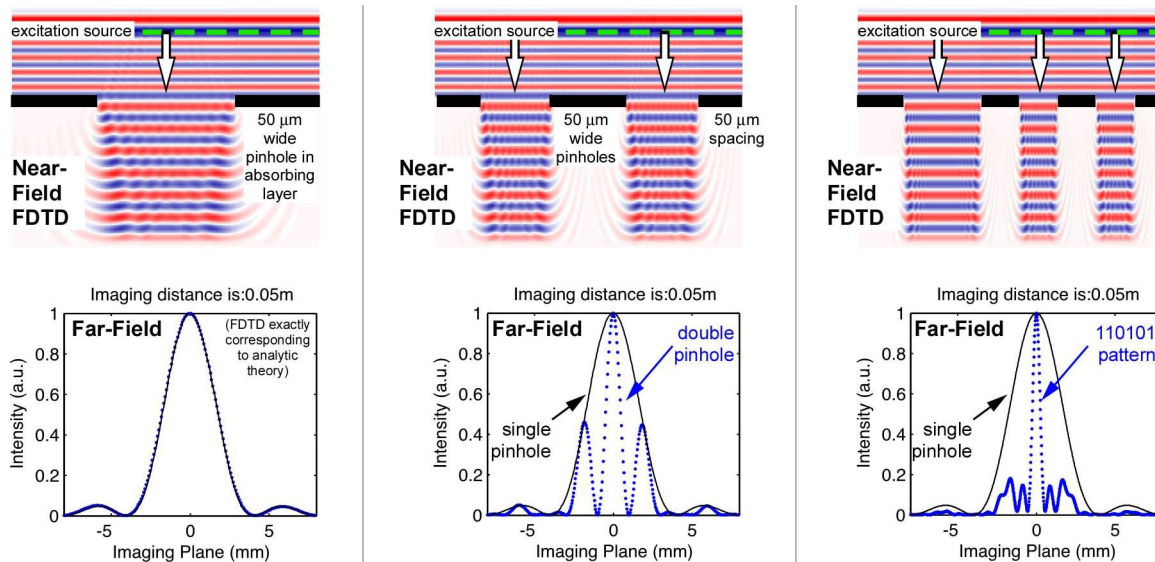


**Figure 6** FDTD calculations of diffraction from an aperture array, using the software WOLFSIM<sup>19</sup> (a) 50 μm aperture and far field pattern, (b) Two 50 μm apertures with classic Young's diffraction pattern, and (c) MRA spacing of four 50 μm apertures with very narrow central lobe and suppressed side lobes .

Figure 7 and Table 2 and show analyses of IR substrate and transparent conductive oxide (TCO) candidates. Currently, the best candidates are Calcium Fluoride (CaF<sub>2</sub>) or Zink Selenide (ZnSe). Figure 7 is a useful plot for comparing the competing optical and electrical parameters of TCO's. In this case, the sheet resistance of the TCO film was fixed at 500 Ω/□, a value commonly used for visible displays. The graph shows the predicted absorption for any  $N$  (carrier concentration) as a function of  $\mu$  (mobility) pair in the MWIR. As a reference, the center of the outlined region is an acceptable absorption (1%). The diagonal lines designate film thickness variations (from <0.1-nm to >10,000-nm). Although CdO appears to be the best candidate, it is a highly toxic material, and therefore InTiO and InMoO are probably better candidates for the application.

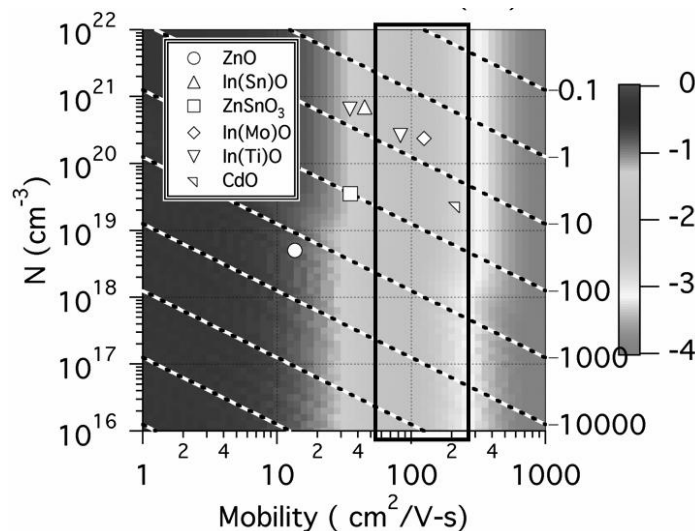


**Figure 7** MWIR absorption of a TCO film with a fixed sheet resistance of 500 Ω/□ (courtesy of J. Perkins, NREL). Materials in box have an acceptable absorption level.

Table 2 Potential MWIR Substrate Candidates

Material	Abbreviation	Visible?	Transmission @4000nm	Hygroscopic?	Temperature	Other
Barium Fluoride	BaF2	Yes	90%	Not until 500OC	500 deg C	
Calcium Fluoride	CaF2	Yes	90-95%	Not until 600OC	600 deg C	
Cleartran	ZnS, multi-spectral	Yes	70%		200 deg C	
Lithium Fluoride	LiF	Yes	90-95%			
Magnesium Fluoride	MgF2	Yes	90-95%	No		Birefringent
Cleartran	spectral	Yes	70%		200 deg C	
Zinc Selenide	ZnSe	above 550nm	60-65%		200 deg C	

#### 4. DAZLE SYSTEM IMPLEMENTATION

The creation of efficient multiplexed DAZLE patterns has a complex constraint space requiring optimization of aperture shape and position constrained not only by MRA or FZP design, but by electrode activation geometry of the LCSLM itself. Furthermore, the desire to multiplex many such patterns in one device creates a novel joint optimization problem (that of pinhole location and size) which can be tackled directly with standard optimization and annealing procedures applied to pseudo-random aperture designs.

Beside the MRA, the Discrete Fresnel Zone Plate (DFZP) has been explored<sup>21</sup> where the FZP is pixelized with a pseudorandom pattern. In similar manner, ArgonST is working with a large number of discrete antenna apertures using Cantor rings as part of the DARPA Novel Satellite Communication initiative. One of the attributes of Cantor rings is that the radii are of fractal dimensions. The Cantor array, like MRAs, is known for its low sidelobe behavior. A similar fractal approach to the DFZP could be invoked which would allow an optimum image plane pattern. Examples of potential aperture designs are shown in Figure 8.

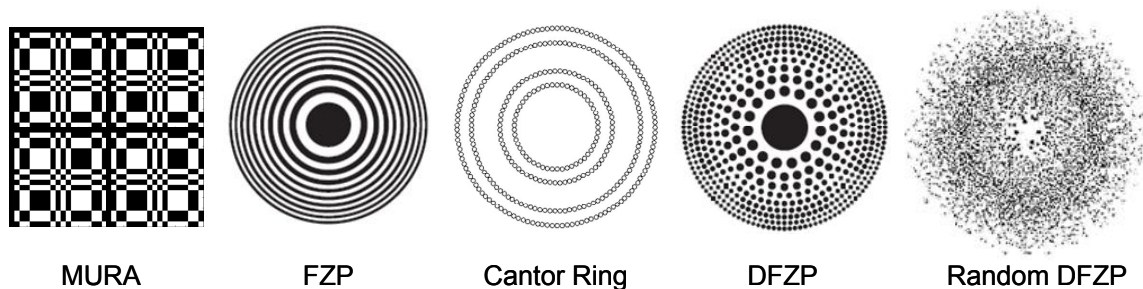
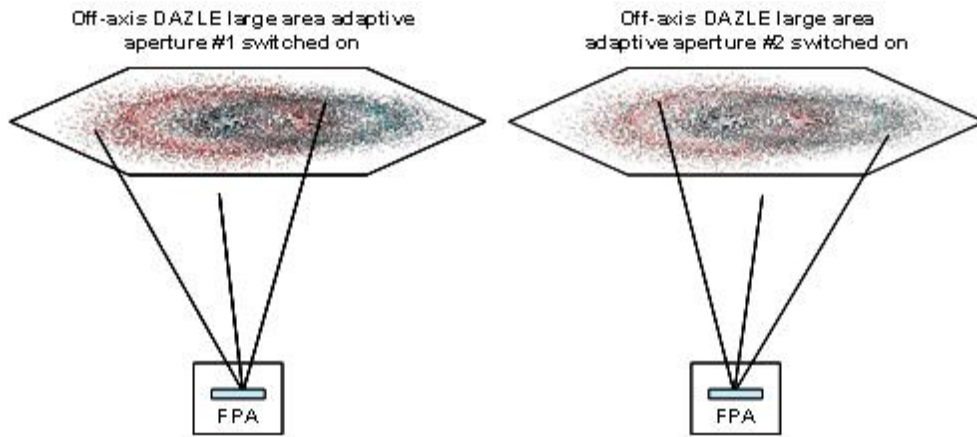


Figure 8 Variations of coded masks, FZP and Cantor Rings

Each pattern of LCSLM aperture array openings creates a different Field Of Regard (FOR) pointing axis. Two of the multiple interwoven DAZLE set of pinhole apertures are schematically shown in Figure 9. This arrangement is similar to other FZP designs<sup>22</sup>, providing a pin-sieve imaging system that allows wide angle, variable resolution imaging. Our

approach, however, depends on large MRA and Cantor ring randomization to minimize MWIR diffraction. The computational challenge is to create off-axis DAZLE arrays such that they provide beam steering while having mostly non-overlapping pinhole apertures connected by simple electrical routing through the electrode surface layers.



**Figure 9** Objective system of interwoven DAZLE apertures covers separate fields of regard

There are many issues concerning the implementation of the DAZLE system including (1) scaling LCSLM size and geometric increase in complexity of aperture element control, (2) LCSLM vibration stability and overall wide-aperture structural design (3) thermal emission from LCSLM versus FOR signal, (4) and wavelength filtering to create coherent light diffractive focusing,

For example, consider the issue of monochromaticity: In addition to diffraction spot size at the FPA, a pinhole array spacing must be designed for a fixed wavelength ( $\lambda_o$ ) within the 3.5-5  $\mu\text{m}$  MWIR band. Wavelengths of light other than  $\lambda_o$  will have slightly altered focal lengths ( $dL_\lambda$ ), creating defocused spot sizes of the order of

$$Spot_\lambda = Diam \left| \frac{dL_\lambda}{L_o} \right| = Diam \left| \frac{d\lambda}{\lambda_o} \right| \mu\text{m}$$

where *Diam* is the DAZLE aperture diameter. The result is a severe limitation on the diameter of any one DAZLE aperture, even with a 1 nm band pass filter as shown in Table 3.

**Table 3** Comparison of Diffraction and Chromatic Spot Size

Objective System imaging at 20 km with 1024x1024 FPA using 20 $\mu\text{m}$ pixels			
Focal Length L = 80 cm, Wavelength bandpass $d\lambda = 1$ nm			
DAZLE Aperture Diameter	IFOV Ground	Diffraction Spot	Chromatic Spot
30 cm	150 cm	0.53 pixels	3.0 pixels
25 cm	125 cm	0.64 pixels	2.5 pixels
20 cm	100 cm	0.80 pixels	2.0 pixels
15 cm	100 cm	1.07 pixels	1.5 pixels
10 cm	100 cm	1.60 pixels	1.0 pixels

The 1 nm filter creates its own set of constraints, limiting the amount of MWIR light that can reach the FPA. If the filter is an integral part of the FPA, then a ground source (with GSD of 1m at 20 km at 355 $^\circ\text{K}$ ) will produce more photons than the LCSLM low temperature black body radiation ( $\sim 275^\circ\text{K}$ ) if both are limited to a 1 nm band-pass (necessary for monochromaticity). Table 4 summarizes the flow of photons through the DAZLE optical system.

**Table 4** DAZLE System Light Flow

Parameter	Value	Units
Irradiance of 1 m Ground Spatial Distance (GSD) at 85°C propagated through atmosphere to 20km height	$1 \times 10^{-12}$	W/cm <sup>2</sup>
Radiant Flux through DAZLE 21cm aperture with 5% open aperture and 99% transmission (not yet filtered)	$1.8 \times 10^{-11}$ $3.7 \times 10^8$	Watts photons/sec
Spot Diffraction for 20 μm pixel with 80 cm FL	15 .76	μm pixels
Spot Blur due Chromatic defocus for band pass $d\lambda = 1$ nm	42 2.1	μm pixels
GSD at 20 km projected onto 20μm pixel FPA	40 2.0	μm pixels
Radiant Flux through DAZLE 40 cm aperture with 5% open aperture, LCSLM 99% transmission, with band-pass of 1 nm	$4.1 \times 10^{-15}$ $8.3 \times 10^4$	Watts/pixel photons/sec/pixel
Background energy from DAZLE aperture itself: Black body at 275°K, with band-pass of 1 nm	$4.8 \times 10^{-16}$ $9.6 \times 10^3$	Watts/pixel photons/sec/pixel
Signal to Noise Ratio in 100 msec integration	86	ratio S/N

Figures 10 and 11 show how DAZLE might look. Each LCSLM aperture plate has a total steerable coverage angle of about 20° using 121 different sets of aperture openings. A total of 37 LCSLM modules mounted on a geodesic structure provide an overall field of view (FOV) of 120°. The MWIR FPA dewars and cooling units are mounted toward the center of the geodesic structure, with heat exhausted to the back.

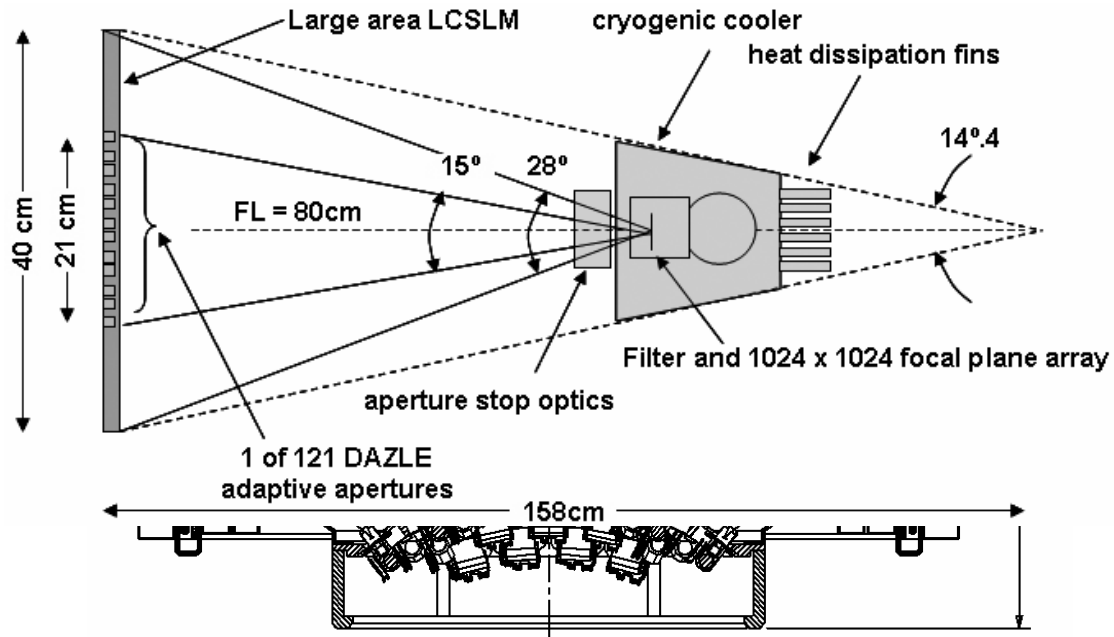


**Figure 10** DAZLE with 37 LCSLM plates on geodesic with corresponding FPA thermal dewars and coolers

**Figure 11** Schematic cross section of one LCSLM module with 121 independent DAZLE pinhole adaptive apertures

## ACKNOWLEDGMENTS

The authors thank Chulwoo Oh for the FDTD simulations, acknowledge productive technical discussions with Steve Serati (Boulder Nonlinear Systems, CO), and thank Frank Gross and Dave Hankins for their simulations and experimental sets for Lena, MURA and FZP analysis.

## REFERENCES

- 1 . DARPA\_SPO, "Large Area Coverage Optical Search-while-Track and Engage (LACOSTE)," Solicitation **BAA 06-11**, 2006.
- 2 . E E Fenimore and T M Cannon, "Coded Aperture imaging With Uniformly Redundant Arrays," *Applied Optics* **17** (3), 337-347 (1978).
- 3 . E E Fenimore, T M Cannon, and E L Miller, "Comparison of Fresnel Zone Plates and Uniformly Redundant Arrays," *Proc. SPIE* **149**, 232 (1978).
- 4 . M J Escuti and W M Jones, "A Polarization-Independent Liquid Crystal Spatial-Light-Modulator," *Proc. SPIE - Optics & Photonics Conference* **6332**, 633222 (2006).
- 5 . M J Escuti, C Oh, C Sanchez et al., "Simplified Spectropolarimetry Using Reactive Mesogen Polarization Gratings," *Proc. SPIE - Optics & Photonics Conference* **6302**, 630207 (2006).
- 6 . C Oh and M J Escuti, "Numerical Analysis of Polarization Gratings Using the Finite-Difference Time-Domain Method," *Physical Review A* **76** (accepted for publication), (2007).
- 7 . R Komanduri, W M Jones, C Oh et al., "Polarization-Independent Modulation for Projection Displays Using Small-Period LC Polarization Gratings," *Journal of the Society for Information Display* **15** (8), 589-594 (2007).
- 8 . G P Crawford, J Eakin, M D Radcliffe et al., "Liquid-crystal diffraction gratings using polarization holography alignment techniques," *Journal of Applied Physics* **98**, 123102 (2005).
- 9 . C Provenzano, P. Pagliusi, and G. Cipparrone, "Highly efficient liquid crystal based diffraction grating induced by polarization holograms at the aligning surfaces," *Applied Physics Letters* **89**, 121105 (2006).
- 10 . C Oh, R K Komanduri, and M J Escuti, "Finite-Difference-Time-Domain Analysis of Polarization Gratings," *Proc. SPIE - Optics & Photonics Conference* **6332**, 633238 (2006).
- 11 . M J Escuti and W M Jones, "Polarization independent switching with high contrast from a liquid crystal polarization grating," *SID Symposium Digest* **37**, 1443-1446 (2006).
- 12 . W M Jones, B L Conover, and M J Escuti, "Evaluation of Projection Schemes for the Liquid Crystal Polarization Grating Operating on Unpolarized Light," *SID Symposium Digest* **37**, 1015-1018 (2006).
- 13 . C Oh and M J Escuti, "Achromatic Diffraction Using Reactive Mesogen Polarization Gratings," *SID Symposium Digest* **38**, L6 (2007).
- 14 . S.D. Kakichashvili, "Polarizational (anisotropic-vectorial) holographic recording on practical photoanisotropic materials," *Optics and Spectroscopy* **42**, 218-220 (1977).
- 15 . L Nikolova and T Todorov, "Diffraction efficiency and selectivity of polarization holographic recording," *Optica Acta* **31**, 579-588 (1984).
- 16 . J. Tervo and J. Turunen, "Paraxial-domain diffractive elements with 100% efficiency based on polarization gratings," *Optics Letters* **25** (11), 785-786 (2000).
- 17 . R Komanduri and M J Escuti, "Elastic Continuum Analysis of the Liquid Crystal Polarization Grating," *Physical Review E* **76** (accepted for publication), (2007).
- 18 . M. Schadt, H. Seiberle, and A. Schuster, "Optical patterning of multi-domain liquid-crystal displays with wide viewing angles," *Nature* **381**, 212-215 (1996).
- 19 . C Oh and M J Escuti, "The Finite-Difference Time-Domain Method for Wideband Analysis of Periodic Anisotropic Media at Oblique Incidence," *Optics Express* **14** (24), 11870-11884 (2006).
- 20 . A T Moffet, "Minimum Redundancy Linear Arrays," *IEEE Transactions on Antennas and Propagation* **AP-16**, 172 (1968).
- 21 . L Kipp, M Skibowski, R L Johnson et al., "Sharper Images by Focusing Soft X-Rays with Photon Sieves," *Nature* **414**, 184-188 (2001).
- 22 . O A Shenderova, *United States Patent Appl. No.* 20050046944 (2005).

- 23 . A L Cohen, *United States Patent No.* 4,338,005 (1982).
- 24 . Y H Fan, H Ren, and S-T Wu, "Electrically Switchable Fresnel Lens Using A Polymer-Separated Composite Film," *Optics Express* **13** (11), 4141-4147 (2005).
- 25 . J C Wiltse and J E Garret, "The Fresnel Zone Plate Antenna," *Microwave Journal* **34**, 101 (1991).